

Svetozar Popovic, Old Dominion University, Norfolk, VA; Milka Nikolic, Old Dominion University, Norfolk, VA;
Janardan Upadhyay, Old Dominion University, Norfolk, VA; Leposava Vuskovic, Old Dominion University, Norfolk,
VA

AIAA-2010-5042

41st Plasmadynamics and Lasers Conference, Chicago, Illinois, June 28-1, 2010

On the Efficient Production of Metastable Oxygen from Electrical Discharges

Svetozar Popović^{* †}, Milka Nikolić[‡], Janardan Upadhyay[§], and Leposava Vušković^{**}
Old Dominion University, Norfolk, VA 23529

We investigate the performance of a cavity microwave discharge (MWD) operating in tandem with a dielectric barrier discharge (DBD). Tandem discharge operates in helium/oxygen mixtures, where metastable molecular oxygen can be produced efficiently using MWD in proportionally large quantities (order of 20% of total oxygen number density). In this new arrangement, DBD provides the metastable-rich mixture to MWD, thereby providing seeding and modifying the discharge kinetics. Both discharges operate in synchronized pulse repetitive mode, which is tailored to maximize power efficiency of the oxygen metastable production. The system operates at pressures up to 350 Torr at average power between 3 to 20 Watt.

Nomenclature

E	=	average electric field
V	=	effective voltage across McCarroll cavity
d	=	effective discharge diameter
α	=	form factor
d_0	=	inner diameter of the tube
Z	=	microwave cavity impedance
P	=	power absorbed in microwave cavity
P_f	=	forward power
P_r	=	reflected power
P_A	=	microwave power factor
Γ	=	reflection coefficient
s	=	standing wave ratio (SWR)
N	=	total average number density
N_x	=	number of exposed O ₂ molecules
N_{O_2}	=	O ₂ number density
N_{SDO}	=	O ₂ (¹ Δ _g) number density
N_{SSO}	=	O ₂ (b ¹ Σ _g ⁺) number density
k	=	Boltzmann constant
T	=	gas-kinetic temperature
p	=	pressure

* Professor, Department of Physics, AIAA Senior Member

† Graduate Student, Department of Physics.

§ Graduate Student, Department of Physics..

** Professor and Eminent Scholar, Department of Physics

W	=	total energy deposited in the discharge
W_0	=	chord
dt	=	time step
v	=	linear velocity of particles in the flow
A	=	tube cross-section area
r	=	O_2/He number density ratio
f	=	total flow rate
f_{HeO_2}	=	flow rate of premixed He/O_2 mixture
f_{He}	=	He flow rate
f_{O_2}	=	O_2 flow rate
Y_{SDO}	=	$O_2(^1\Delta_g)$ yield
Y_{SSO}	=	$O_2(b^1\Sigma_g^+)$ yield

I. Introduction

OXYGEN molecule has seven long-living metastable states located in the energy diagram below the first dissociation limit, at 5.1eV, approximately. Most interesting are the three singlet states, $a^1\Delta_g$ (Oxygen Singlet Delta – OSD), $b^1\Sigma_g^+$ and $c^1\Sigma_u^-$ (Oxygen Singlet Sigma – OSS). Transition from the singlet states to the oxygen ground state, $^3\Sigma_g^-$, represents a magnetic dipole transition (singlet-triplet intercombination). Hence their low transition probability and long life time: more than 2000 s for OSD, and 3 to 7 s for OSS (See Table I)¹. Rather difficult to observe by conventional spectroscopy techniques, these states, especially the OSD, have become of increased interest due to their reactivity and important role in a variety of environments, experiments and applications². OSD ($a^1\Delta_g$) is the lowest electronically excited state of molecular oxygen with 0.977 eV above the ground state $X^3\Sigma_g^-$ and its most efficient production would occur in discharges where the average electron energy is about 1 eV. It turns out that average electron energy of 1 eV usually occurs at the reduced field values of about 10 Td. Unfortunately, most self-sustained and the e-beam sustained discharges operate at substantially higher reduced electric fields and/or average electron energies. In most cases, the electrons are able to excite higher energy levels of the molecular oxygen, such as $B^3\Sigma_u^-$ or $A^3\Sigma_u^+$ which will then collisionally decay into another metastable state, $c^1\Sigma_u^-$ or to the long-lived $A^3\Delta_u$ state. All these states have dissociation energy less than 1 eV and could undergo thermal dissociation to form the ground state, $O(^3P)$, or the metastable state, $O(^1D)$. OSD is not present at kinetic temperatures above 2000 K where most of the oxygen is dissociated or reacted. Second prominent member of this group is OSS ($b^1\Sigma_g^+$). Its lowest vibrational state is about 1.63 eV above the ground state, which is within the average energy range of electrons in most electrical discharges. Hence, electrical discharges can easily produce all molecular oxygen metastables and two atomic metastable states. This provides a strongly reactive mixture that has not always a well adjusted kinetics for a particular application.

List of possible atomic and molecular transitions that could be used in the detection of metastable oxygen using optical emission spectroscopy is given in Table II. They include magnetic-dipole allowed atomic and molecular transitions and double/binary (dimole) emission.

Table I - Oxygen metastable states and their radiative lifetimes

O ₂ species	O species	E (eV)	τ (sec)[1]
a ¹ Δ _g (SDO)		0.979	2700
b ¹ Σ _g ⁺ (SSO)		1.630	7
c ¹ Σ _u ⁻		4.058	25-50
C ³ Δ _u		4.264	5-50
A ³ Δ _u			
A ³ Σ _u ⁺		4.349	0.16-0.25
⁵ Π _g			
	¹ D		114
	¹ S		0.84

Table II - List of dipole-forbidden and dimole transitions (arranged by increasing wavelength)

Transition	Designation	Band origin (cm ⁻¹)	Wavelength nm	Energy eV	Obs.
A ³ Σ _u ⁺ → X ³ Σ _g ⁻	Herzberg I	35010	286 nm	4.349	
A ³ Δ _u → X ³ Σ _g ⁻	Herzberg III	34387	291 nm	4.272	
c ¹ Σ _u ⁻ → X ³ Σ _g ⁻	Herzberg II	32665	306 nm	4.058	
A ³ Δ _u → a ¹ Δ _g	Chamberlain	26346	380 nm	3.273	
c ¹ Σ _u ⁻ → a ¹ Δ _g		24776	404 nm	3.078	
a ¹ Δ _g ⁺	binary	20010	476 nm	2.486	+
b ¹ Σ _g ⁺ → 2X ³ Σ _g ⁻					
c ¹ Σ _u ⁻ → b ¹ Σ _g ⁺		19543	512 nm	2.428	
2 a ¹ Δ _g → 2X ³ Σ _g ⁻	dimole	17240	580 nm	2.142	+
¹ D → ³ P	atomic	15872*	630.03 nm	1.972	+
2 a ¹ Δ _g → 2X ³ Σ _g ⁻	dimole	15750	634 nm	1.957	+
2 a ¹ Δ _g → 2X ³ Σ _g ⁻	dimole	14220	703 nm	1.767	+
b ¹ Σ _g ⁺ → X ³ Σ _g ⁻	Atmospheric	13122	762.08 nm	1.630	+
a ¹ Δ _g → X ³ Σ _g ⁻	IR Atmospheric	7889	1267.59 nm	0.978	
b ¹ Σ _g ⁺ → a ¹ Δ _g	Noxon	5233	1910.95 nm	0.649	

For illustration, one molecular, one atomic and a dimole transition are shown in Figures 1a,b The dimole transition is clearly visible, but rather weak and diffuse. On the other hand, the atmospheric band is remarkably strong, especially in the post-discharge interval between two microwave pulses. Therefore, time resolved spectroscopy could be used to obtain spectroscopic analysis of gas temperature and b state density from relative intensities of rotational lines and from absolutely calibrated integral spectrum of the b ¹Σ_g⁺(v = 0) → X ³Σ_g⁻(v = 0) band. Absolutely calibrated emission spectroscopy was also used to estimate concentration of O(¹D) since the ¹D →

3P transition was readily seen at 630.03 nm near the pulse end and up to about 200 μ s after. OSD concentrations were determined by cavity ring down spectroscopy in the arrangement involving MWD only.

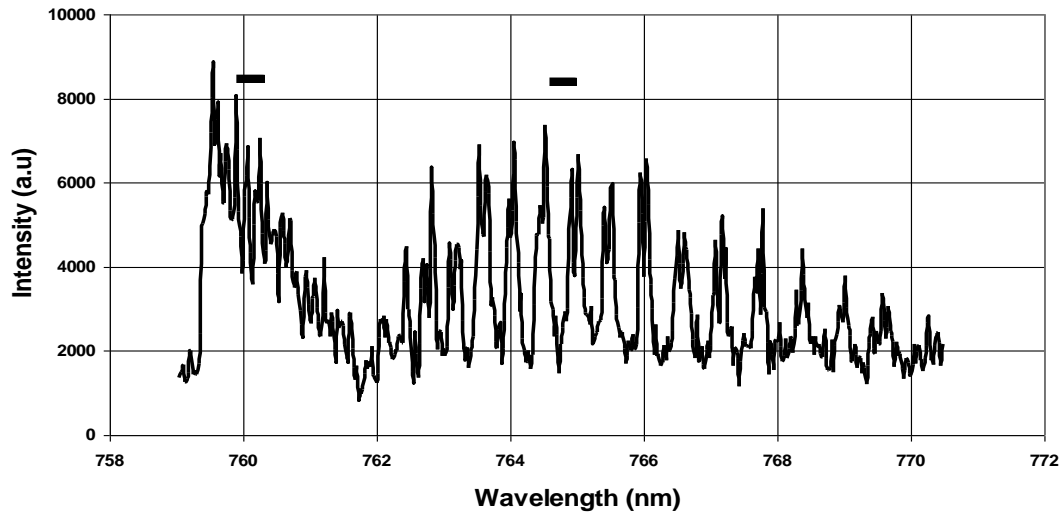


Figure 1a. $b^1\Sigma_g^+ \rightarrow X^3\Sigma_g^-$ “atmospheric” band showing strong presence of OSS in the post-discharge region. Discharge conditions: $p = 300$ torr, average MW forward power 12 W, average MW reflected power 0.5 W, pulse repetition rate 1000pps, square-wave, pulse duration 300 μ s; DBD voltage 3 kV; flow rate 40 sccm, 97% He 0.1% O_2 . Spectrum was observed side-on starting at 50 μ s after the pulse end, with a gate of 50 μ s. RR and RQ branches are located between 759 and 762 nm. And PP and PQ branches are extended from 762 to over 770 nm.

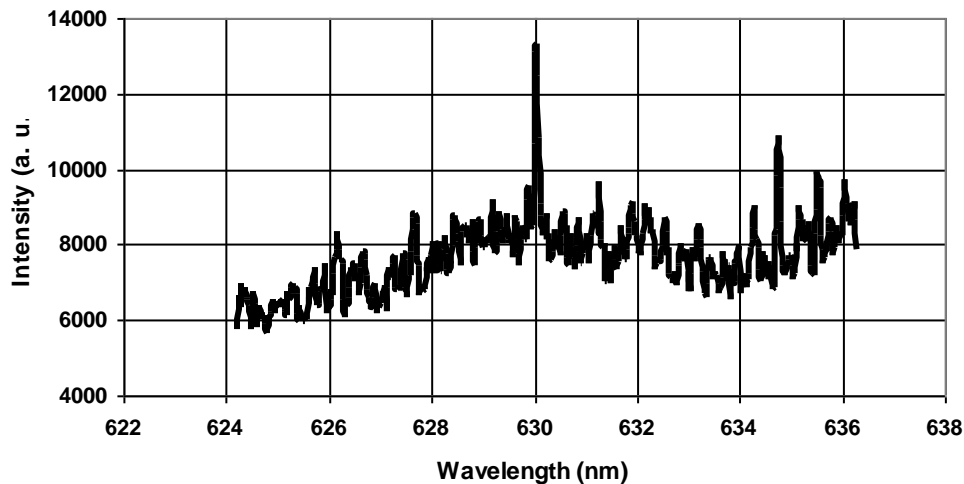


Fig. 1b. Blue wing of a broad dimole radiation with the band origin around 634 nm is sometimes accompanied by the atomic oxygen $^1D \rightarrow ^3P$ line at 630.03 nm. Discharge conditions: $p = 30$ torr, average MW forward power 6 W, average MW reflected power 0.5 W, pulse repetition rate 1000pps, square-wave, pulse duration 300 μ s; DBD voltage 3 kV; flow rate 40 sccm, 97% He 3% O_2 . Spectrum was observed end-on at 50 μ s after the pulse end, with a gate of 100 μ s.

In the following sections, we will describe the DBD and MWD separately, and their operation in tandem configuration. We will also discuss the reduced electric field, average deposition energy and metastable oxygen yields as the scaling parameters of MWD operating per se or in tandem with DBD. Diagnostic techniques used will be briefly described and arguments for their use will be discussed in the following section. Last section before

conclusion will cover and analyze the experimental results and discuss scaling possibilities for high pressure operation.

II. Tandem Discharge

A. Dielectric Barrier Discharge

Scheme of the dielectric barrier discharge used in tandem with MWD is given in Figure 2, which was described in more detail by Leiweke and Ganguly³. In Figure 2 it is presented in the individual operation mode. Quartz tube wall is the dielectric barrier between the anode, located inside the tube, and grounded cathode, located outside the tube. A CMOS switch defined the pulse repetitive operation of DBD. The switch was triggered by a pulse generator, which was controlled by the pulse from MW generator, which acted as a master clock.

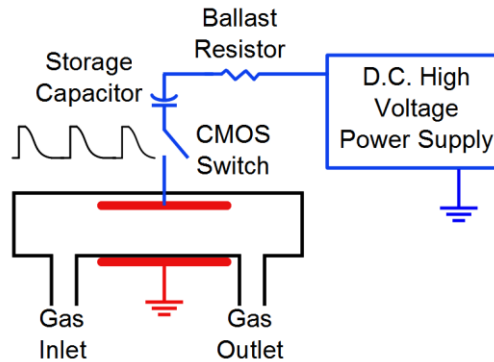


Figure 2. Scheme of the DBD

In its short pulse version, with voltage rise-time of 10 ns, and pulse duration up to 100 ns, this discharge was capable of producing large concentration of metastable states, while operating in pure Ar, as shown in Fig. 3. This property holds for any gas mixture, which we have already observed by the seeding effects DBD has on the downstream MWD. Detailed analysis of the flow of metastables through the DBD post-discharge section is still being made and we are not yet able to state definite composition of the MWD provided by DBD. Robust concentration of Ar metastables shown in Fig,3, indicates potential for strong effects on MWD kinetics.

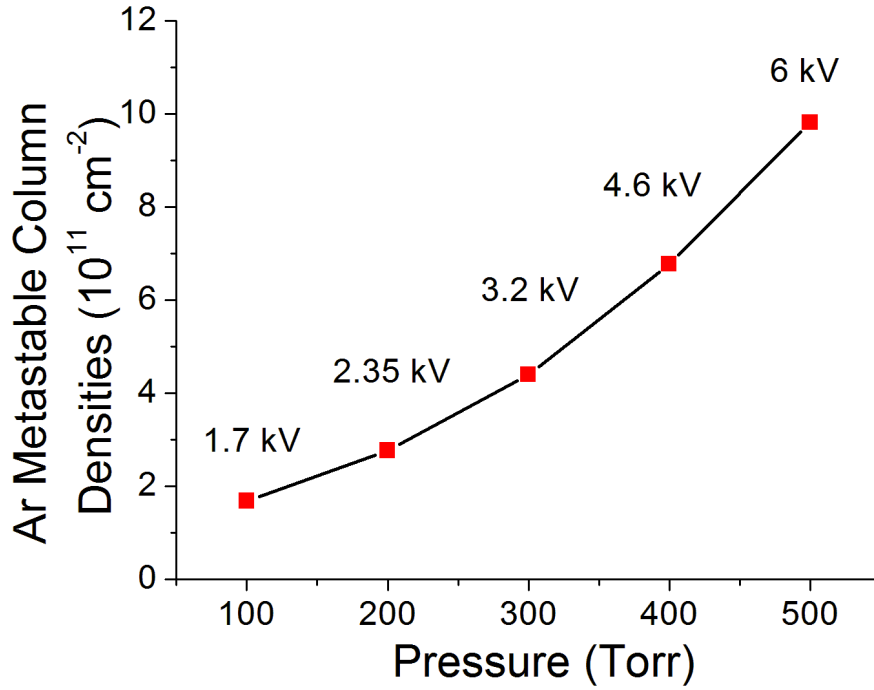


Figure 3. Ar metastable column density increase with pressure in the DBD operation as individual unit ³

B. Microwave Cavity Discharge

McCarroll cavity discharge in cw operation mode has been already successfully used for metastable oxygen production and detection^{4, 5, 6}. This discharge seemed to have a convenient electron density and temperature distribution to fit conveniently into specific energy requirement for OSD production. In most types of discharges, average reduced electric field exceeds value of around 10 Td, which is widely considered to provide maximum metastable state population⁷. In the microwave discharges the reduced electric field covers the range between 1 and 100 Td. To illustrate this we are using the simple estimate of reduced electric field obtained from the measured discharge parameters.

Average electric field across the half-inch tube in an Evenson cavity can be evaluated from the measured of forward and reflected power using the following relations:

$$\begin{aligned}
 E &= \frac{V}{d} \\
 V &= \sqrt{PZ} \\
 Z &= Z_0 \frac{1+\Gamma}{1-\Gamma} = Z_0 s \\
 P &= P_f - P_r = P_f (1-\Gamma^2) \\
 \Gamma &= \sqrt{\frac{P_r}{P_f}}
 \end{aligned} \tag{1}$$

where E is the average electric field, V is the effective voltage across McCarroll cavity, $d = \alpha d_0$, d_0 is the diameter of the tube, α is the form factor of the discharge – a number lower than one, P is the power absorbed by the discharge, given as the difference between forward power P_f and reflected power P_r , Z is the impedance of the cavity with the discharge, $Z_0 = 50\Omega$, s is the standing wave ratio, and Γ is the reflection coefficient. The form factor is based on the distribution of the electric field across the tube, which is a combination of TM mode (along the tube axis) and the surface wave mode (across the tube). In this configuration, the actual plasma resembles a partially filled ellipsoid shell. At lower pressures, the shell is mostly filled and is practically homogeneous. At higher pressure, the surface plasma structure appears more enhanced. Without going in to many details on the discharge morphology, for present purpose we take an average form factor value of 0.8, evaluated for pressure range of 50 to 300 Torr, and absorbed power range of 10 to 100 W.

Depending on conditions, the reflection coefficient Γ was between 0.1 and 0.7 in present experiment, the standing wave ratio was between 1.2 and 6, and the average electric field between 20 and 90 V/cm. In this simple approach we can estimate the average reduced electric field as the ratio of the average electric field E in the cavity and the average number density in the discharge N :

$$\frac{E}{N} = \frac{VkT}{pd} = \frac{(1+\Gamma)kT\sqrt{Z_0P_f}}{pd} \quad (2)$$

expressed in the terms of measured quantities – discharge temperature T , reflection coefficient Γ , forward power P_f , and pressure p , where k is Boltzmann constant. For present experimental analysis the Eq. (2) is conveniently transformed into

$$\frac{E}{N} = 0.0259 \times \frac{T}{273} \times \frac{760}{p} \times \left(1 + \sqrt{\frac{P_r}{P_f}}\right) \times \sqrt{P_f} \quad (3)$$

where E/N is expressed in Td (10^{-17} Vcm²), T in K, p in Torr, and P_f , P_r in W. Formula for the reduced electric field is further simplified into

$$\frac{E}{N} (\text{Td}) = 0.072 \times \frac{T(\text{K}) \times \tilde{P}_A(\sqrt{W})}{p(\text{Torr})} \quad (4)$$

where

$$\tilde{P}_A = \left(1 + \sqrt{\frac{P_R}{P_F}}\right) \times \sqrt{P_F}$$

is MWD power factor. For illustration, pressure dependence of E/N based on measured pressure and temperature is given in Figure 5. According to these data we can conclude that the optimum reduced electric value (~ 10 Td) is crossed between 10 and 50 Torr in the power range between 20 and 100 W. For the higher pressure operation more power has to be delivered into the discharge.

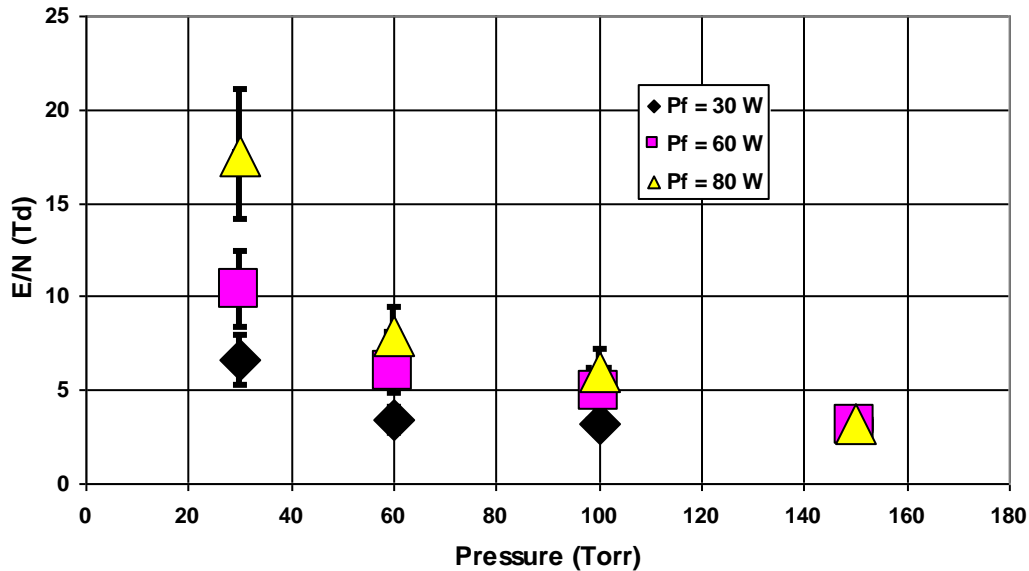


Figure 4. Reduced electric field evaluated from formula given in Eq. (4). Evaluation was made using temperature data obtained from the OSS spectrum (0-0 atmospheric band). This procedure will be discussed later in the text. Discharge conditions: MWD in cw operation; $f=100$ sccm; 97% He/ 3% O₂; DBD voltage 1.5 kV; DBD repetition rate 1000 pps.

C. Tandem Discharge

Our first goal in this work was to inspect the possibility to increase the yield of OSD in the oxygen content of discharge mixture by inducing transition to this state by collisional/radiative recombination from the high-energy oxygen states including other metastables and ozone. So far, all discharge-based techniques for production of OSD relied on the excitation intensive mechanisms whereby the discharges were designed so that rate of OSD production is obtained at minimum energy cost. Nevertheless, large concentrations of ozone and other metastables have escaped the plasma reactor. This led not only to the energy losses, but also to the complexity that these other species brought into the OSD chemistry.

In order to accomplish this task we combined DBD and MWD to share the same flow tube. The immediate plan was to study the possibilities of tailoring DBD so to enhance quenching of other metastables, reduce overall energy loss by reducing the breakdown conditions, and generate substantial ultraviolet radiation for photodissociation of ozone. The second goal was readily fulfilled and increased dramatically the pressure range of operation in MWD. It opened so many possibilities that we had to reduce temporarily our program just to the study the effect of the increased pressure range.

The tandem discharge tube is shown schematically in Figure 5. Two discharges are arranged in a sequence. Upstream discharge is a short-pulse (~50 ns, voltage rise-time 10 ns) dielectric barrier discharge with the anode located inside the tube. This section of the tube is of rectangular cross-section so that the discharge is diffuse and relatively homogeneous, extending for about the length of the anode at pressures higher than 30 Torr. Microwave cavity discharge is generated in the commercial McCarroll cavity discharge (Ophos), located 8 cm downstream. The tube section occupied by the MWD and its post-discharge is 30 cm long. Side-on observations were made through the slit on the cavity's short circuit plate and at various locations along the post-discharge section. End-on observations were made through two quartz windows at both ends of the tube. Gas flow was directed from the port upstream of DBD through both discharges to the end of the MWD's post-discharge section. Two additional gas ports are located in the post-discharge section of the DBD to provide inflow for atomic-oxygen quenching gas (CO₂ in present work) and for other reactive gases.

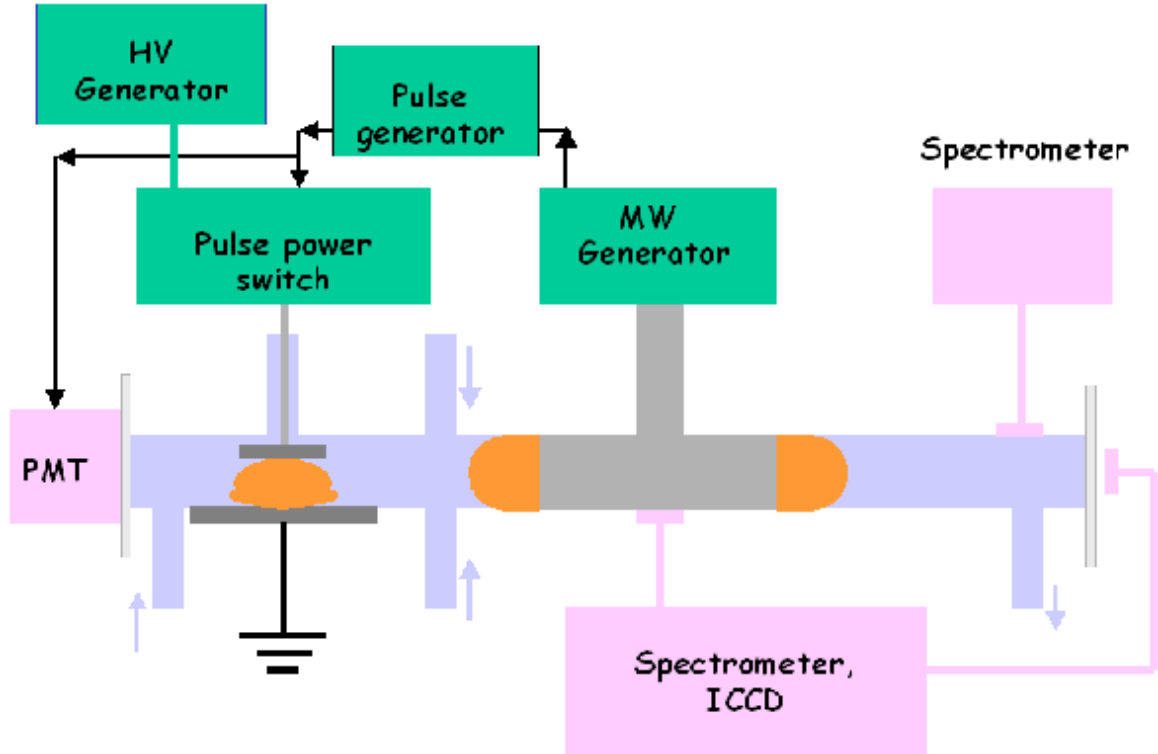


Figure 5. Scheme of the experimental setup for the tandem discharge operation and diagnostics

DBD was supplied by a Glassman 20-kV generator, although only up to 7.5 kV was used in this work. MWD was supplied by an Ophos modulated Microwave generator (maximum power 100 W). Triggering of DBD and the time-resolved diagnostic tools was made using a pulse generator, where the modulated square-wave signal from MW generator was used as the master clock. Both discharges operated at repetition rate close to 1 kHz, dictated by the limited frequency range of MW generator. Pulse generator regulated triggering of the filtered photomultiplier tube (PMT) and ICCD (Princeton Instruments). PMT was used to observe time-resolved spectral lines from DBD. A high-resolution spectrometer (Acton) with the ICCD was used to record post-discharge spectra of the metastable oxygen features by side-on and end-on observation. Side-on observation was used for temperature diagnostics in the discharge section (in post-discharge time windows), and end-on viewing had longer observation path, suitable for recording of weak, metastable radiation. Additional low-resolution spectrometer (Ocean Optics) was used to record spectrum in wide wavelength range - 200-900 nm. Observed radiation was transmitted to detectors with UV-visible-near-infrared fiber optic cables. All time-resolved detection systems were calibrated using a Spectra Physics blackbody irradiance source.

III. Diagnostic Techniques

A variant of the cavity ring down spectroscopic technique, the off-axis integral cavity optical spectroscopy (ICOS) was used to quantitatively detect the $a^1\Delta_g$ state of O_2 via the hitherto unobserved (1,0) band of the $b^1\Sigma_g^+ - a^1\Delta_g$ Noxon system. This approach allows for the quantitative detection of singlet O_2 with a minimum detectable density of 4×10^{13} molecule cm^{-3} at 298 K corresponding to 3×10^{12} molecules per cm^{-3} per quantum state. Off-axis ICOS is convenient because it allows narrowband, continuous-wave lasers to be used in conjunction with optical cavities in a simple and effective manner^{8, 9}. The absorption signal is obtained through the temporal integration of the laser intensity transmitted through the cavity in the same fashion as in conventional absorption measurements. The absorption due to the medium inside the cavity is determined from the cavity output, i.e. laser transmission, which is a function of the mirror reflectivity as well as scattering and absorption losses between the mirrors⁹.

The afterglow from the OSD-generating plasma (microwave discharge in the McCarroll cavity) passed through a coupling and through the off-axis ICOS measurement system at about 3000 sccm and a variable total pressure. Coupling device is either a quartz tube with or without a frit, or a 5 cm Teflon® tube. Frit was used to filter out water molecules and OH radicals⁵. The off-axis ICOS system consisted of an 82-cm long high-finesse

optical cavity bounded by two highly reflective mirrors ($R=99.9986\%$). The mirror reflectivity was determined by performing a cavity-ring down measurement¹⁰. Ring down time constant is up to $250\ \mu\text{s}$ (see Fig. 6). The exact laser frequency and tuning rate are determined by using known water absorption features and a calibrated SiO_2 etalon. The ambient water spectrum is taken after the off-axis ICOS cell is filled with about 5 Torr of ambient laboratory air. The lines appearing in the spectrum are easily assigned to known water transitions using the HITRAN96 database¹¹. Diode laser output is tuned by changing the temperature of the case to the wavelength range of a particular transition between the rotational levels of the Q branch of the Noxon $a^1\Delta_g \rightarrow b^1\Sigma_g^+$ (1,0) band. In addition, the laser output was fine-tuned over 2 GHz frequency range in order to scan the Doppler and pressure-broadened rotational lines. This was accomplished by supplying a saw-tooth current ramp to the laser current source, while holding the laser case temperature constant. For calibration purpose, beam is directed prior and after the set of spectral measurements through a fused-silica etalon. Repetition rate of the saw-tooth pulse (laser wavelength tuning rate) is always kept at least an order of magnitude smaller than the characteristic cavity frequency. However, too low repetition rate distorts the symmetry of the line profile. This effect is observed in most recorded line profiles, but the error due to line profile distortion could be reduced to less than 2% by choosing carefully the sweep parameters. A typical

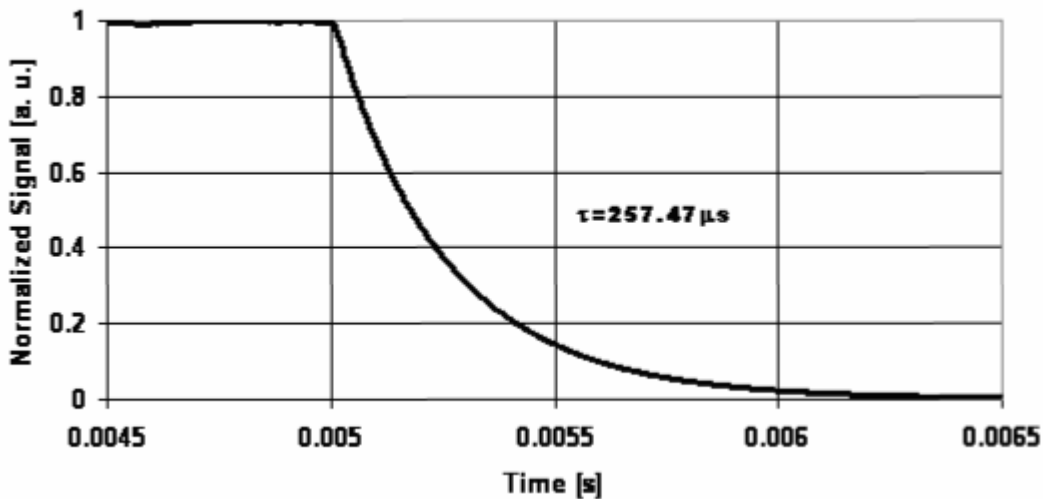


Figure 6: Ringdown signal waveform in the off-axis ICOS system⁵.

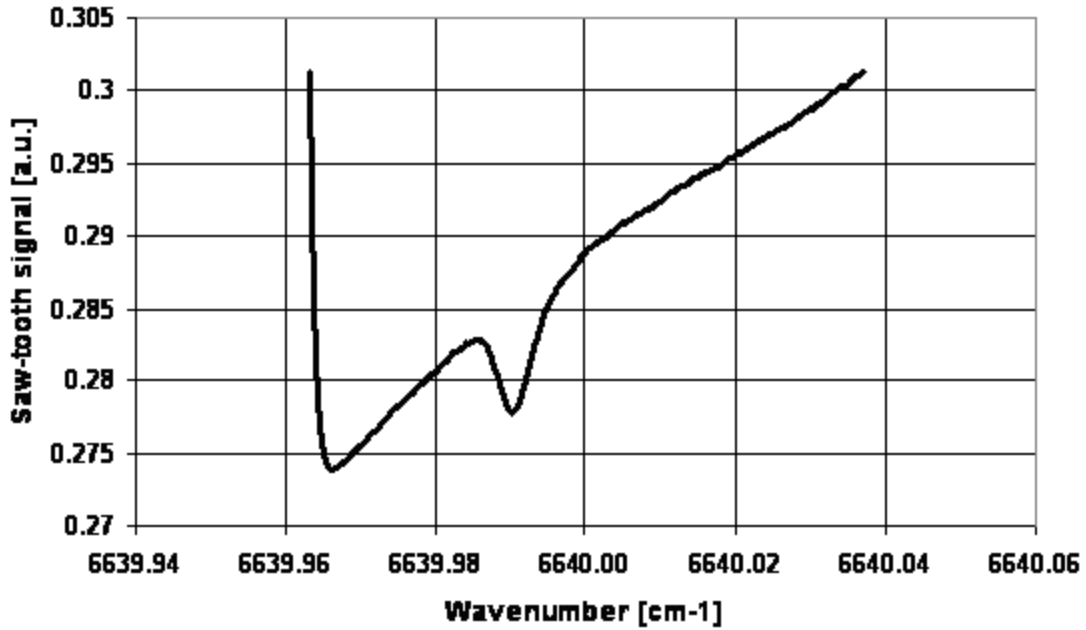
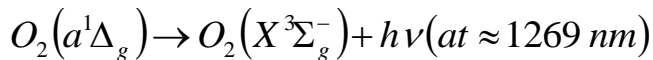


Figure 7: A rotational line from Noxon band as observed with help of the sweep tuning of the semiconductor laser⁵.

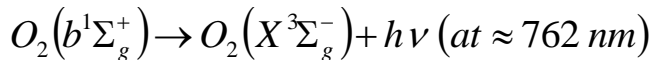
absorption line shown in Fig. 7 was fitted with Voigt profiles using the approximate procedure derived by Whiting¹².

Besides the diagnostics of OSD, special emphasis was given to the relative density of atomic and molecular states, which indicate the particle kinetics in the discharge. Following the ideas implemented in Ref. 5, we are developing a link between simpler atomic-molecular optical emission spectroscopy (OES) and the OSD production. Primary OES diagnostics was to detect and monitor emission from metastable oxygen based on the following reactions:

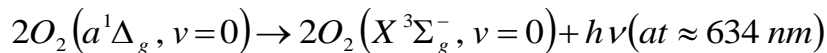
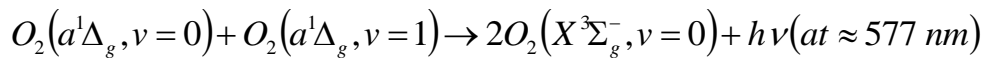
- Radiative decay of OSD

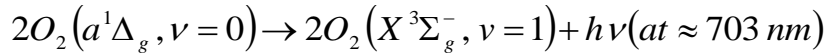


- Radiative decay of OSS



- Spontaneous emission from OSD complex (dimole radiation)





All of these radiation bands, except for the vibrationally excited OSD complex have been already observed in electrical discharges⁷, mostly in long ducts or drift tubes.

Secondary OES diagnostics is related to the spectroscopic determination of gas temperature, which is important for accurate determination of the reduced electric field from Eq. 4. The most common spectroscopic technique is based on the use of small amount of nitrogen and observation of a rotational band belonging to the Second Positive System ($C^3\Pi_u \rightarrow B^3\Pi_g$). The observed spectrum of a band is compared with synthetic spectrum where temperature is the only free parameter. This technique assumes equilibrium of rotational lines within a vibrational band and also the reproduction of the same equilibrium in the ground state upon the electron impact excitation of the C state. This assumption may be severely violated in the presence of strong atomic population, by the energy transfer from excited atoms to selected rotational lines in the system. In addition, chemical reactions may produce additional cascading excitation that result in strong populations of short-lived energetic excited nitrogen molecules. This effect results apparent two- or multi-temperature distribution of rotational states neither of which could be assigned to gas kinetic temperature.

As we have shown in Figure 1a, the $b^1\Sigma_g^+ \rightarrow X^3\Sigma_g^-$ transition from OSS to ground state is rather strong and clear from most interfering spectral features in MWD. This long-living state is a more reliable object for spectroscopic determination of temperature, because a negligible amount is lost or created by chemical reactions during the time window of observation. The spectrum is composed of two branches, R and P, each having two subbranches RQ, RR, PP and PQ. R and P branches are shown in Figure 8a and 8b in a finer resolution. During the discharge, the spectrum is somewhat distorted by oxygen short-lived bands, but only 50 μs after the pulse ends the spectrum is clear and more suitable for temperature diagnostics. We assume that the gas temperature could not drop substantially in that time interval. Average rate of temperature decay in post-discharge measured by this method was 1K per 10 μs , which indicates that the using of a time window (gate 50 μs) delayed by 50 μs from the end of the discharge would result in temperature several degrees lower.

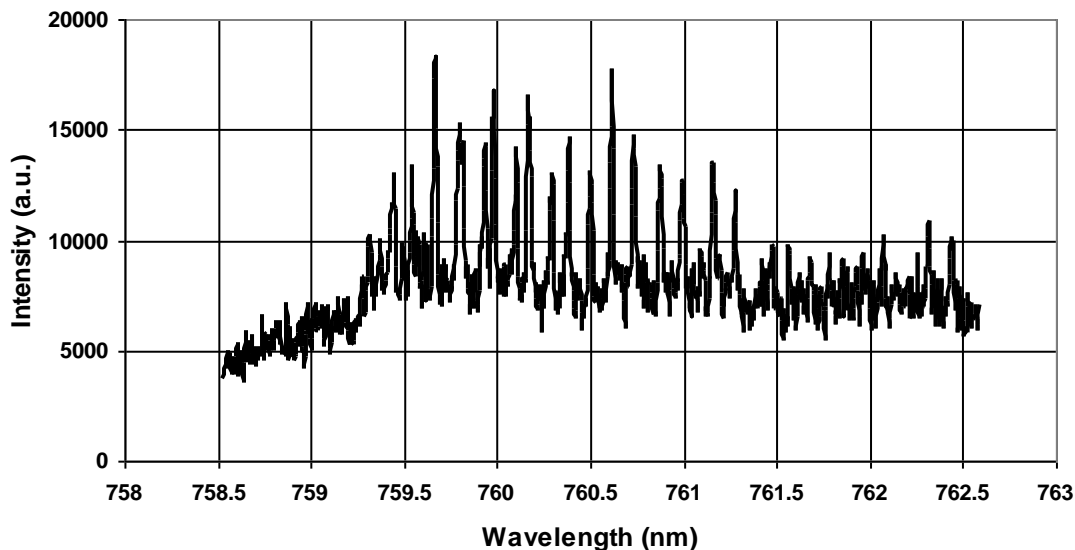


Figure 8a. RR and RQ branches of the atmospheric band $b^1\Sigma_g^+ (\nu=0) \rightarrow X^3\Sigma_g^- (\nu=0)$ recorded by end-on observation of the MWD post-discharge: repetition rate 1000 pips; pulse duration 300 μs ; average forward power 12 W; DBD: voltage 2.5 kV, repetition rate 1000 pips; 0.4% O_2 , 99.6% He, pressure 30 Torr; Time window: delay 300 μs ; gate 600 μs .

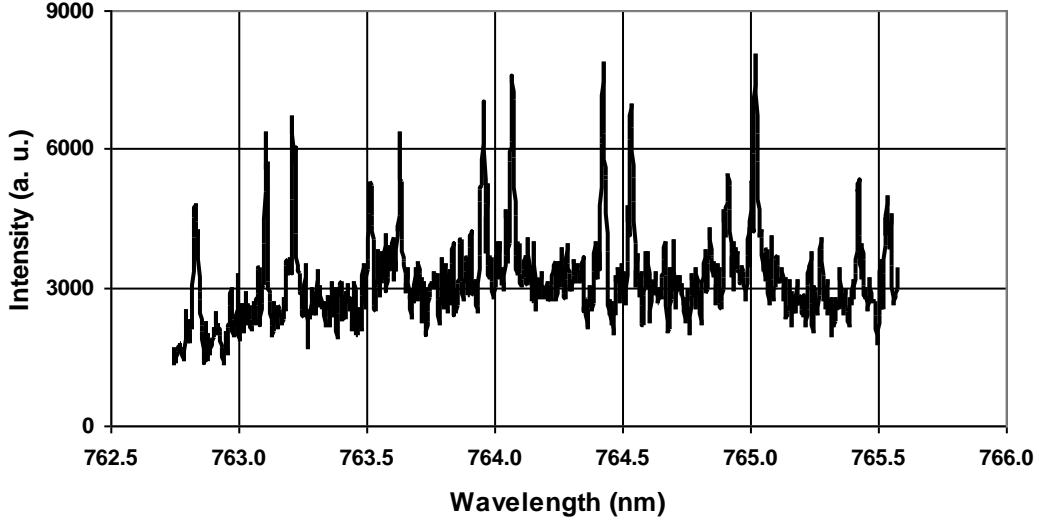


Figure 8b. Rotational lines belonging to the PP ($J = 4, 6, 8, 10, 12, 14, \text{ and } 16$) and PQ branch ($J = 6, 8, 10, 12, 14, \text{ and } 16$) of the atmospheric band $b^1\Sigma_g^+ (v=0) \rightarrow X^3\Sigma_g^- (v=0)$ recorded at identical conditions as in Fig. 5a.

Temperature was determined by observation of the above spectra side-on at the center of MWD in a time window $50 \mu\text{s}$ long starting with $50 \mu\text{s}$ delay after the pulse. Rotational constants and partition functions were taken from Ritter and Wilkerson¹³. In most cases only the lines of PP branch were used, but the discrepancy with PQ branch was less than 5%.

Energy per oxygen molecule is considered to be an important parameter in analyzing the optimum conditions for electric discharge-based production of OSD. In the following we will expose briefly the evaluation of the deposited energy for the Evenson/McCarroll cavities that we used in our previous work. By definition

$$W_o = \frac{W}{N_x}, \quad (5)$$

where W_o is the energy per oxygen molecule in J, W is the total energy deposited into discharge during a given time interval Δt , and N_x is the total number of exposed oxygen molecules. One can substitute

$$\begin{aligned} W &= P\Delta t \\ N_x &= N_{O_2} v\Delta t A \end{aligned}, \quad (6)$$

where P is power absorbed by the discharge, N_{O_2} is the number density of oxygen molecules, v is the total linear velocity in the gas flow, and A is the cross-section area of the discharge tube. Therefore,

$$W_o = \frac{P}{N_{O_2} vA}. \quad (7)$$

Total number density of oxygen atoms is given in terms of measured pressure, temperature, and flow rates as

$$N_{O_2} (\text{cm}^{-3}) = 2.687 \times 10^{19} \times \frac{p(\text{Torr})}{760} \times \frac{273}{T(\text{K})} r = 9.652 \times 10^{18} \frac{p(\text{Torr})}{T(\text{K})} r \quad (8)$$

where r is the number density ratio of oxygen molecules. In one part of this work we have used oxygen diluted in helium in the proportion 20:80 so that

$$r = \frac{0.2 f_{\text{HeO}_2}}{f_{\text{He}} + f_{\text{HeO}_2}} = 0.2 \frac{f_{\text{HeO}_2}}{f}.$$

where the flow rates of helium/oxygen mixture, f_{HeO_2} , and of helium, f_{He} , are given in sccm. Otherwise, r is obtained by the simple ratio of the oxygen and total flow rates. Linear velocity of molecules in the mixture flowing through the discharge is given by

$$v(\text{cm/s}) = \frac{f(\text{cm}^3/\text{s})}{60} \times \frac{T(\text{K})}{273} \times \frac{760}{p(\text{Torr})} \times \frac{1}{A(\text{cm}^2)} = 0.0464 \frac{f(\text{cm}^3/\text{s}) \times T(\text{K})}{p(\text{Torr}) A(\text{cm}^2)} \quad (9)$$

Total number density of singlet O_2 ($^1\Delta$), N_{SDO} , is obtained by deconvolution and integration of the broadened absorption line from the Noxon band in the cavity ringdown waveform. Total number density, N_{SSO} , of singlet O_2 ($^1\Sigma_g^+$) was evaluated comparing the blackbody irradiation source intensity recorded with the same apparatus as used for recording the radiation of the atmospheric band $b^1\Sigma_g^+ \rightarrow X^3\Sigma_g^-$. Total yields are then calculated from

$$Y_{\text{SDO}} = \frac{N_{\text{SDO}}}{N_{\text{O}_2}} = N_{\text{SDO}} \frac{kT}{p} \frac{f_{\text{O}_2} + f_{\text{He}}}{f_{\text{O}_2}} = 1.036 \times 10^{-19} N_{\text{SDO}} \frac{T}{p} \frac{f}{f_{\text{O}_2}} \quad (10a)$$

$$Y_{\text{SSO}} = \frac{N_{\text{SSO}}}{N_{\text{O}_2}} = N_{\text{SSO}} \frac{kT}{p} \frac{5(f_{\text{HeO}_2} + f_{\text{He}})}{f_{\text{HeO}_2}} = 5.18 \times 10^{-19} N_{\text{SSO}} \frac{T}{p} \frac{f}{f_{\text{HeO}_2}} \quad (10b)$$

where the pressure p is given in Torr, temperature T in K, and flow rates $f, f_{\text{O}_2}, f_{\text{HeO}_2}$ in sccm.

IV. Results

In Fig. 9 is shown the distribution of average temperature along the MWD. It shows that in our relatively narrow parameter range the temperature remains roughly constant. There are fine details related to the influence of DBD discharge, manifested in slightly elevated temperature in the upstream section. Also, local measurements indicate the possibility of small departure from laminar flow which would result in higher residence times and increased quenching processes. These subjects is will be the matter of future study, which may result in a different construction of microwave cavity and more careful synchronization between DBD and MWD.

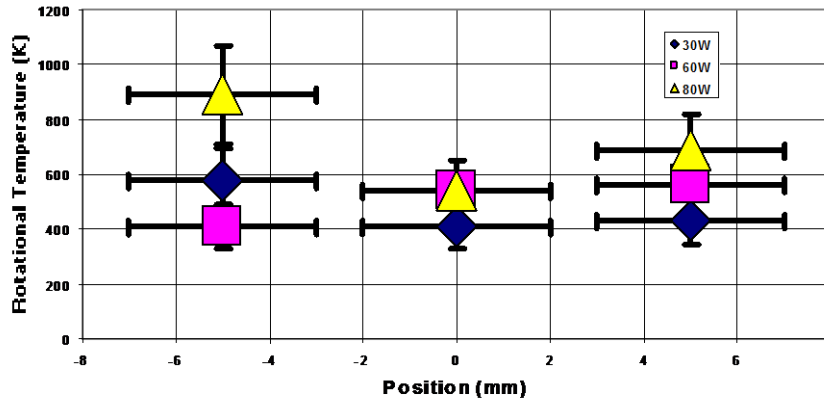


Figure 9. Temperature distribution along MWD discharge

Figure 10 shows the OSD yield as a function of the reduced electric field, defined by Eq. (10a). Data on oxygen-“rich” and oxygen-“lean” mixtures show clear distinction. Oxygen-“lean” mixtures show high yield and tendency of saturation or a broad maximum around 15 Td. They are scattered much more than the average experimental error, most probably due to higher contribution of impurities at low flow rates of oxygen. Oxygen-“lean” mixtures show growing trend, much lower scattering and continuity of yield value at 150 and 300 sccm. Part of our current work is to elucidate the discrepancy between the “lean” and “rich “ mixtures. Operation at high pressure in the tandem discharge is allowing for a more intensive study. .This analysis is not yet complete and will be reported elsewhere.

Results indicate that the maximum yield is shifted by about 3 Td with respect to the established theoretical predictions ($E/N \sim 11$ Td). Reason for this discrepancy can be found in the possibility that the MWD form factor is closer to unity for the “lean “ mixtures. MWD in the “rich” mixtures is more electronegative, due to higher concentration of oxygen, and evaluation of its form factor is rather complex. This is still a useful information that has to be addressed in future work.

Absolute value of the yield is less doubtful since the errors were estimated conservatively, using standard methods for evaluation of density from the absorption lines. The main error in the yield value is introduced by errors in temperature measurements, which are likely to be improved in near future.

Figure 11 shows the OSS yield as evaluated from Eq. (10b) based on the absolute irradiance measurements of the rotational lines of the R branch of the $b^1\Sigma_g^+ (v=0) \rightarrow X^3\Sigma_g^-(v=0)$ transition. Although absolute values are still under scrutiny, the location of the maximum was tested at other gas mixtures..

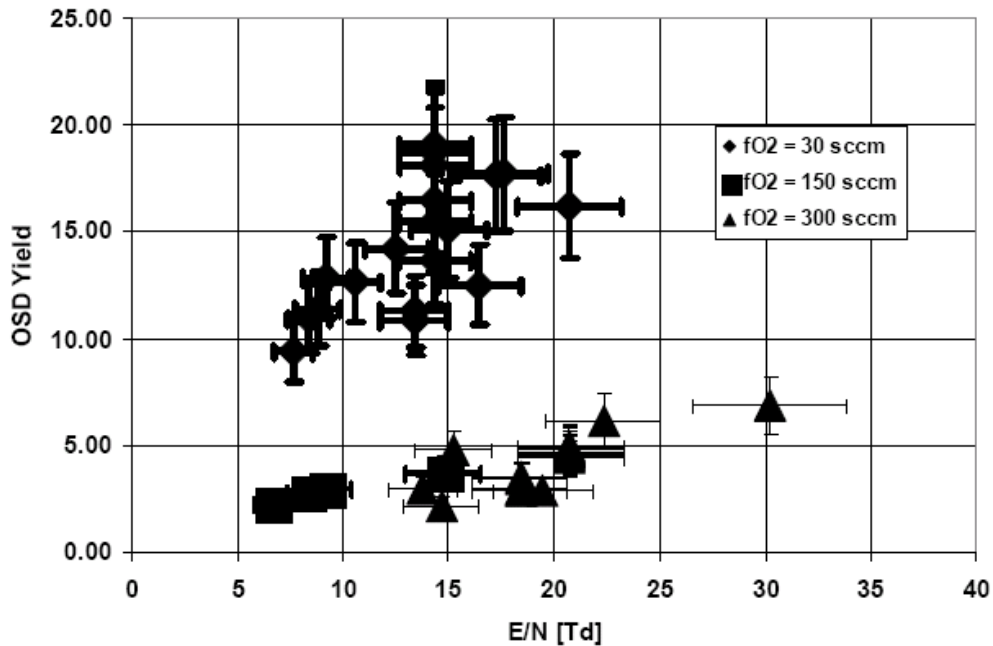


Figure 10. Results for $O_2(^1\Delta_g)$ yield measurements using off-axis ICOS method illustrate different behavior of Oxygen “lean” and “rich” mixture with Helium.

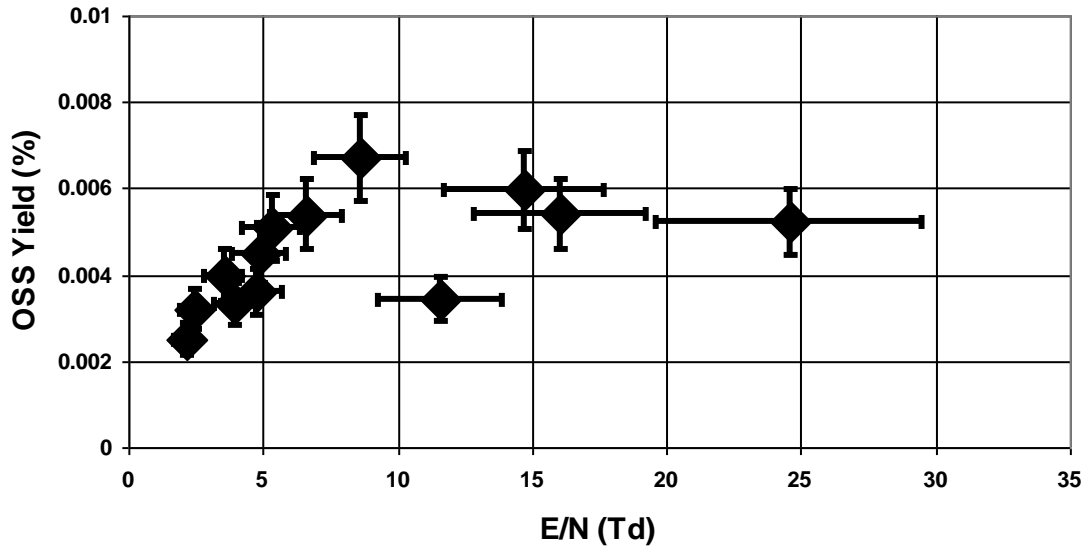


Figure 11. Results for the $O_2(^1\Sigma_g^+)$ yield evaluated from absolute intensity measurements of rotational lines in the R branch of the atmospheric band. Gas mixture consisted of 3% Oxygen and 97% He.

V. Conclusion

Maximum yield of OSD obtained in this experiment was as much as 19%. This yield is by more than a factor 2 higher than the yield reported previously for microwave cavity discharges. We propose several reasons for this discrepancy. First, in-situ emission spectroscopy relies on very low emission signals, and numerous sources could augment the measurement error. On the contrary, the ICOS technique relies on a very long absorption path, measured in kilometers, stable conditions in the cell, relatively far away from the discharge to be affected by possible fluctuations induced by high temperature of gas particles in the discharge. Second, emission data could not take into account the amount of OSD or any solid obstacle in the flow. Therefore, the additional production in the afterglow is not compensated by any decay and the population seems to be constantly added as long as there are other metastable species in the system. Third, in present work, the diluting gas was helium, which is known to enhance internal energy storage into oxygen, and the range of oxygen content was much wider.

Tandem discharge in the described configuration offers a unique possibility to eliminate ionization penalty often present in electrical discharges and thus to increase their energy efficiency when used as chemical reactors. Present example supports this case by demonstrating sustained operation in He/O₂ mixtures at average power below 20 W and at pressure of 350 Torr. The experiment was clearly power limited and the power upgrade of the system is clearly needed. Scaling parameters for holding the reduced electric field strength in the optimum range are known. Concentration of atomic oxygen in the system has to be decreased in order to stabilize production yield and discharge volume, and to eliminate depletion by collisional quenching at elevated pressure.

Acknowledgments

Authors gladly acknowledge support and discussions with Drs. Biswa Ganguly, Skip Williams and Robert Leiweke, WPAFRL, and the staff of Hanscom and WP AFRL for the support during S. Popović's Summer Faculty Fellowship tenures.

References

- ¹ Slanger T. G. and Copeland R. A., “Energetic Oxygen in the Upper Atmosphere and the Laboratory”, *Chemical Review*, **103** (2003) 4731–4765.
- ² Carroll D L, Verdeyen J T, King D M, Zimmerman J W, Laystrom J K, Woodard BS, Benavides G F, Kittel K, Stafford D S, Kushner M J and Solomon W C, “Continuous-wave laser oscillation on the 1315 nm transition of atomic iodine pumped by O₂(a¹Δ) produced in an electric discharge,” *Appl. Phys. Lett.* **86** (2005)111104 (3 pages).
- ³ Leiweke RJ and Ganguly BN, “Effects of pulsed-excitation applied voltage rise time on argon metastable production efficiency in high pressure dielectric barrier discharge,” *Applied Physics Letters*, **90** (2007) 241501 (3 pages).
- ⁴ Rawlins W T, Lee S, Kessler W J and Davis S J, “Observations of gain on the I(²P_{1/2} → ²P_{3/2}) transition by energy transfer from O₂(a¹Δ_g) generated by a microwave discharge in a subsonic-flow reactor,” *Appl. Phys. Lett.* **86** (2005) 051105.
- ⁵ Popović S, Rašković M, Kuo S P and Vušković L, “Reactive oxygen emission from microwave discharge plasmas,” *Journal of Physics: Conf. Ser.* **86**, (2007) 012013.
- ⁶ Williams S., Popovic S., Gupta M., “Microwave plasma generation and filtered transport of O₂ (a¹Δ_g),” *Plasma Sources Science and Technology*, **18**, (2009). 035014.
- ⁷ Smirnov VV, Stelmakh OM, Fabelinsky VI, Kozlov DN, Starik AM, and Titova NS, “On the influence of electronically excited oxygen molecules on combustion of hydrogen–oxygen mixture,” *Journal of Physics D: Applied Physics*, **41** (2008) 192001.
- ⁸ Paul J B, Lapson L and Anderson J G, “Ultrasensitive Absorption Spectroscopy with a High-Finesse Optical Cavity and Off-Axis Alignment,” *Appl. Opt.* **40**(2001) 4904-4910.
- ⁹ O’Keefe A, Scherer J J and Paul J B, “CW integrated cavity output spectroscopy,” *Chem. Phys. Lett.* **307** (1999) 343-349.
- ¹⁰ Baer D S, Paul J B, Gupta M and O’Keefe A, “Sensitive absorption measurements in the near-infrared region using off-axis integrated-cavity-output spectroscopy,” *App. Phys. B* **75** (2002) 261-265.
- ¹¹ Rothman L S, Rinsland C P, Goldman A, Massie S T, Edwards D P, Mandin J -Y, Schroeder J, Mc-Cann A, Gamache R R, Wattsin R B, Yoshino K, Chance K V, Juck K W, Brown L R, Nemtchechin V and Varanasi P, *J. Quant. Spec. Radiat. Transf.* **60** (1998) 665-710.
- ¹² Whiting E E, “An empirical approximation to the Voigt profile,” *J. Quant. Spec. Radiat. Transf.* **8** (1968)1379-1384.
- ¹³ Ritter KJ and Wilkerson TD, “High-resolution spectroscopy of the oxygen A band,” *J. Mol. Spectr.*, **121** (1987) 1-19.